The Conceptual Design of a Tailless Sailplane Having a Stabilizing Fuselage

Ippei Otani and Mark D. Maughmer
Department of Aerospace Engineering
The Pennsylvania State University
University Park, Pennsylvania 16802
mdm@psu.edu

Abstract

A conceptual design of a tailless Standard Class sailplane is presented in this paper. Longitudinal static stability requires a negative pitching moment gradient with respect to the lift coefficient and a positive pitching moment at zero lift. The former depends on the position of the center of gravity with respect to the neutral point of the aircraft, while the latter, in the case of tailless sailplanes, is obtained by designing the wing to take over the stabilizing function normally provided by the empennage. The two methods employed to achieve this, often in combination, are the use of an airfoil with a positive moment coefficient about its aerodynamic center, and the aft sweeping with washout of the wing to provide the needed positive pitching moment at zero lift. The idea introduced here explores a fuselage design that helps to support the stabilizing function. The pressure distribution around the fuselage is tailored to contribute to the stability of the vehicle. To determine the overall benefit of this concept, the cross-country performance of the tailless aircraft is predicted and compared to that of a current conventional sailplane. It is found that the conceptual design is predicted to achieve performance levels comparable to those of conventional designs.

Nomenclature

$\bar{c}$	mean aerodynamic chord
C_D	drag coefficient
C_{DPfuse}	pressure drag coefficient of the fuselage
C_L	lift coefficient
C_{Lfuse}	lift coefficient of the fuselage
C_{Lmax}	maximum lift coefficient (aircraft)
c_{lmax}	maximum lift coefficient (airfoil)
C_{Lreq}	required lift coefficient for turn
C_{Ltrim}	trim lift coefficient
C_M	moment coefficient
C_{mac}	moment coefficient about the aerodynamic center (airfoil)
C_{Mnp}	moment coefficient about the neutral point
C_{Mo}	moment coefficient at zero lift
C_{Mofuse}	moment coefficient of the fuselage at zero lift
D	drag
D_f	skin friction drag
d	ground distance
h	altitude difference
i_{fuse}	local incidence angle of fuselage camberline
k_2-k_1	fuselage fineness ratio
L	lift
L_{req}	lift required
l_{fuse}	length of fuselage
l_{VT}	moment arm of vertical tail
M	moment
M_{NP}	moment about neutral point
m	mass of aircraft
NP	neutral point of aircraft
R	turn radius
Re_{fuse}	Reynolds number of fuselage
S	reference area
S_{VT}	vertical tail reference area
S_W	wing planform area
V	airspeed
V_{ACC}	average cross-country speed
V_c	climb velocity
V_g	glide velocity
V_S	sink velocity
$V_{sink\ turn}$	turning sink rate
V_{turn}	turning velocity
V_{trim}	trim velocity
V_{VT}	vertical stabilizer volume
W	weight
w_{fuse}	average width of fuselage section
x	longitudinal displacement of center of gravity from the neutral point
x_{cg}	chordwise location of the center of gravity
α	angle of attack
α_{ow}	angle of attack of the zero-lift-line relative to the fuselage reference line
Δx	length of fuselage increments
δ_{elev}	elevon deflection angle
Λ_{wing}	wing sweep angle
ρ	atmospheric density
ϕ	bank angle

Introduction

Since the early days of the successful flights of Lilienthal and the Wrights, various overall configurations have been considered by airplane designers with the objective of

increasing performance and efficiency.[1-2] The configuration that has predominated has been that having an empennage positioned at the end of a tail boom of some length, providing a moment arm aft of the main wing.[1-2] A different design approach is one without the tail boom and empennage.[1, 3-4] At first glance, such a design appears promising for reducing drag, as significant portion of the non-lifting components of the aircraft are eliminated.

Unfortunately, as a result of the wing taking over the stability and control functions of the tail, the attainment of a high maximum lift coefficient and low drag are adversely affected such that, in many cases, the gain obtained by eliminating the tail boom is negated.[2-3, 5] One of the reasons for this is that, for the vehicle to have positive static stability, the airfoils used on tailless configurations must have a small, or positive, moment coefficient about the aerodynamic center. As this limits the amount of aft loading that can be utilized, the maximum lift coefficient achievable by such airfoils is compromised. This results in an increased wing area being needed for low-speed operation, which largely offsets the reduced drag benefit achieved by eliminating the tail boom, although recent advances in airfoil design have lessened this disadvantage to some extent.[2, 6] Historically, while some tailless sailplanes fulfilled their mission requirements satisfactorily,[7-8] it is still generally advantageous from the aerodynamic point of view to have an empennage, even though this increases the wetted area of the non-lifting components.[3] Nevertheless, the knowledge base on tailless aircraft is still relatively small and additional research may lead to new successful solutions.[1-2] The current project, named *H02g*, further explores the concept by considering the conceptual design of a tailless Standard Class competition sailplane.

Static longitudinal stability requirements

The conditions for an airplane to be longitudinally statically stable and trimmable are a negative pitching moment derivative with respect to lift and a positive pitching moment coefficient at zero lift.[9] That is,

$$\frac{\partial C_M}{\partial C_L} < 0 \qquad (1)$$

and

$$C_{Mo} > 0 \qquad (2)$$

The first condition is satisfied by positioning the center of gravity in front of the neutral point of the aircraft.[9] The second condition is more challenging for tailless designs.[2] In conventional configurations, the horizontal tail mounted with a negative incidence angle relative to the wing creates a downward force at zero lift and, with the tailboom acting as a lever arm, produces a positive pitching moment.[9] In the absence of the tail, the wing has to provide the necessary moment. One method of accomplishing this uses an airfoil with a positive pitching moment about the aerodynamic center, as achieved by using an airfoil having a reflexed camberline.

Reflexed airfoils have been traditionally of lower performance than the conventional ones, due to the fact that having a pressure distribution that produces a positive moment coefficient is at odds with the achievement of high lift and low drag.[2] Recent developments in airfoil design, however, have made possible the development of laminar airfoils with a positive or a small negative moment coefficient at the aerodynamic center, and performance that is more comparable to conventional ones.[2, 6]

Another method for attaining longitudinal static stability is to sweep the wings aft and include washout along the wingspan. The resulting difference between the local angles of attack at the root and the tip, which are also separated in the longitudinal direction due to the sweep, creates a nose-up pitching moment for the entire aircraft at zero lift.[2, 9]

The stabilizing fuselage

For the *H02g*, the feasibility of using a stabilizing fuselage is explored. Such a fuselage has a pressure distribution that results in a nose-up pitching moment, thus creating a positive zero-lift pitching moment C_{Mo} and helping to reduce the adverse effects of the traditional approaches explained above.[2] A prone position for the pilot was chosen over the conventional seated position. Three-dimensional panel method results have demonstrated that a prone position results in the fuselage shape having the most favorable pitching-moment characteristics.

The design process began with conceptual ideas for the stabilizing fuselage, which were then analyzed using the three-dimensional, low-order panel code, *DWT*.[10] This was the main tool used for predicting the overall aerodynamic characteristics of the *H02g*, while the primary tool used for designing the wing geometry was a multiple lifting-line code.[11] An iterative process led to a wing design satisfying the requirements of low stall speed and low drag. Once the geometry of both the fuselage and the wing was fixed, the wing/body combination was analyzed to determine the static longitudinal stability parameters. The neutral point and the moment coefficients were calculated to ensure the viability of the design. Once a configuration displayed longitudinal static stability, its performance was evaluated. The multiple lifting-line code was again used to calculate the spanwise lift distribution and induced drag. The airfoil profile drag properties of the wing were predicted using the two-dimensional airfoil analysis capability of the software package, *XFOIL*.[12] The final outputs of the entire evaluation process are the speed polar diagram and the average cross-country speed calculated over a selected range of thermal strengths. These results were then compared with those of the Schempp-Hirth *Discus 2*, a modern competitive Standard Class racing sailplane.[13]

Configuration and aerodynamic design

Sizing and weight estimation

The first step in the conceptual design of the *H02g* was sizing and weight estimation. As there were no unconventional weight saving technologies incorporated into this new design, the weight estimation process relied on historical trends.[2, 14] For the fuselage, a weight between that of the tailless design of Akaflieg Braunschweig, the *SB13*, and that of other tailed sailplanes is thought to be a reasonable estimation, noting that the absence of the tailboom does not amount to as much weight savings as might be expected.[15] Using this information, the fuselage weight is taken to be 100 *kg*.

The wing weight estimation had to account for the increased torsion moment due to the sweep that is necessary to provide a moment arm for the vertical tails situated at the wingtips. Following other examples,[14] an inverse power function was found that uses the cosine of the sweep angle as the argument. This function is an approximation for the weight increase due to the sweep over conventional straight wings. The other parameter that has an influence on the wing weight is the planform area.[2] The formula used for estimating the wing weight is given by,

$$W_{Wing} = (11.312 \cdot S_W{}^2 - 215.4 \cdot S_W + 1142) \cdot \cos(\Lambda_{Wing})^{-10.936} \qquad (3)$$

The gradually increasing sweep angle of the crescent-like wing is approximated by the sweep angle of the line connecting the quarter chords at the root and tip. Given that the *H02g* has a wing area of 10.0 m^2, and the sweep angle of the line connecting the quarter chords lines at the root and the wingtip is 9.3 degrees, the wing weight is estimated to be 137.8 kg. Adding the fuselage weight plus 90 kg, due to the pilot and other equipment, to that of the wing, the overall gross weight of the *H02g* without water ballast is 328 *kg*. In addition, once the geometry of the wing was defined, it was determined that the wing volume is sufficient for carrying 200 liters of water ballast.

The sizing of the sailplane wing is dictated by the rules of the Standard Class, as well as certification regulations. Taking safety into consideration, the minimum speed was taken to be comparable to that of other designs, 73 km/h. The resulting wing area of 10.0 m^2 provides a reasonable compromise between a light wing loading needed for climbing in weak conditions and a high wing loading for good performance in strong weather conditions.[2, 16] To enclose the necessary equipment, landing gear, and pilot, the fuselage length was set to 3.85 m.

Fuselage design

The design of the stabilizing fuselage was begun by examining the pitching moment of the fuselage using the following approximation given by Multhopp's formula,[17-19]

$$C_{Mofuse} = \frac{k_2 - k_1}{36.5 S\bar{c}} \sum_{x=0}^{x=l} w_{fuse}^2 (\alpha_{ow} + i_{fuse}) \cdot \Delta x \qquad (4)$$

In considering the quantities that could make a positive contribution to the pitching moment at zero lift, the correction factor for the body fineness ratio (k_2-k_1) and the average width of the fuselage section (w_{fuse}) could not be altered significantly from typical values without having a detrimental effect on the performance. The term i_{fuse} refers to the local incidence angle, that is, the angle between the fuselage camberline and the longitudinal axis. It is defined as positive when the fuselage camber of the portion in front of the wing is oriented in the nose-up direction, and that part aft of the wing drooping downward.[21] The fuselage was configured so that this quantity is positive. As shown in Fig. 1, this is achieved by shaping the mold line that runs along the widest portion of the fuselage to curve upwards as it approached the nose of the airplane from below the wing root.

The primary purpose of the fuselage aft of the wing is to avoid flow separation rather than to obtain a positive pitching moment contribution. During the process of exploring ideas using the panel method software, it was also found that a cross sectional shape of a polygon with rounded corners rather than the more typical elliptical shape helps to increase the nose up moment. The last variable, α_{ow}, is the angle of the wing zero lift line with respect to the fuselage reference line.

The prone piloting position

In conventionally configured sailplanes, the pressure distribution pattern on the fuselage results in the lowest pressures being in the vicinity of the wing root, close to where the center of gravity and neutral point are located. In designing a fuselage to have a positive pitching moment, the objective was to move the upper-side, low-pressure region forward. This led to the adoption of the prone position for the pilot, as presented in Fig. 2. The success of this approach can be observed in Figs. 3 and 4, in which the region of low pressure near the pilot's head results in a fuselage that is predicted to have favorable stabilizing characteristics. Such a pressure distribution on the fuselage allows for the use of airfoils having negative c_{mac} values, without relying on wing sweep and twist.

The comfort and safety of the prone position are not easy to assess since aircraft accommodating pilots in such a fashion are rare. Nevertheless, flight-test reports on the Horten flying wing series indicate that the unorthodox seating arrangement had won the approval of experienced test pilots, even after a number of several-hour-long flights.[1] The pilot in the *H02g* will have the upper body supported by a 20 degree slope relative to the horizontal fuselage reference line, while that of the Horten sailplanes had an angle of about 30 degrees. In spite of the pilots' approval of the prone position even on several-hour-long flights, it is acknowledged that further investigation into the ergonomic and crashworthiness aspects is necessary to establish the feasibility of this unusual seating

posture. One possible disadvantage may be the fact that the pilot has to turn his or her neck to a further extent than is usually the case to check for traffic above and behind the sailplane. The grazing angle, which is the angle between the canopy surface tangent line and the pilot's line of vision, was established so that it had roughly the same value as that of existing conventional designs, that is, about 20 degrees. The canopy itself was also expanded behind the pilot's head to widen the field of view rearward.

Aerodynamic analysis of the fuselage

The aerodynamic characteristics of the fuselage without the wings were predicted. Using the *DWT* panel method, the fuselage by itself produces only a moment couple as a result of its pressure distribution. It does not produce any significant amount of lift. The wing alone is expected to generate to the required lift. It is unstable by itself since it uses an airfoil profile with a very small but negative c_{mac} value. The moment coefficient of the fuselage at an angle of attack corresponding approximately to that of cruise (–2.0 degrees), referenced to the wing area and mean aerodynamic chord length, is approximately +0.028.

In addition to establishing the stabilizing characteristics of the fuselage, computations were carried out in order to ensure that excessive flow separation does not occur. This was done using a feature of the panel method package that calculates the skin friction coefficient along the on-body streamlines, and predicts separation using two-dimensional boundary-layer analysis along the streamlines.[10] The results shown in Fig. 5 indicate that near the stalled flight condition, separation occurs only over the last few percent of the body.

Wing design

The wing planform geometry was determined using the multiple-lifting-line code of Horstmann.[11] The dihedral needed for lateral stability was given essentially a parabolic curvature as predicted to minimize induced drag.[20] The actual amount used for the *H02g*, however, was approximated from the values used on production sailplanes. In order to take advantage of the absence of a tail boom, vertical fins are placed at the wingtips as was done on the *SB13* sailplane. This solution should increase the span efficiency by allowing the tail surfaces to serve as winglets, resulting in both favorable handling and improved performance. The effectiveness of these surfaces is improved by gradually sweeping the wing aft to provide a moment arm.

The constant-chord elevons are situated at the trailing edge of the wing and extend along its entire span. This was done to minimize the deterioration of the span efficiency due to control surface deflections, which generally alters the lift distribution, and also to avoid the addition of wetted area due to a devoted elevator, as found on Fauvel and Marske tailless sailplanes.[1] The *HO2g* planform is shown in Fig. 6. Its k-factors, predicted using the Horstmann code and presented as they depend on lift coefficient in Fig. 7, are found to be reasonably low.

Due to the limited availability of high-performance sailplane airfoil profiles that satisfy the requirement of very small or positive value of c_{mac}, an airfoil suitable for this design study was obtained with the help of *XFOIL*.[12] The resulting airfoil, shown in Fig. 8, uses the camberline of the Wortmann FX05H-126 and a thickness distribution that is an interpolation of those of the Wortmann FX66S-171 and the HQ36K/15.12. The predicted moment coefficient and the drag polar for this airfoil are presented in Figs. 9 and 10. From these results, it is evident that modern airfoils with small moment coefficients can achieve drag characteristics that are comparable to those having more conventional camberlines.

Vertical tails

As the benefit of designing a new airfoil for the vertical tails would be minimal, the FX71-L-150/30, as used on Standard Class gliders of the 1980's, was chosen as the starting point for this effort.[2] This airfoil is linearly morphed into a modified PSU90-125 airfoil at the tip of the winglet/vertical fin to improve drag characteristics at low Reynolds numbers that is a consequence of the narrowing chords toward the tips of the vertical surfaces. While this project does not go deeply into issues of lateral/directional stability of the aircraft, the vertical tail is sized such that the vertical tail volume, given by

$$V_{VT} = \left(\frac{\partial C_L}{\partial \alpha} \right)_{VT} \cdot l_{VT} \cdot S_{VT} \qquad (5)$$

is same or a greater than those of existing successfully flying tailless gliders.[1-2, 8] The vertical tail volume for the *H02g* is shown along with values of other tailless sailplanes in the same class in Table 1.

Stability and control

In the case of tailless aircraft, stability and control are closely related to the overall performance, since both depend almost entirely on the wing.[2] For example, a change in longitudinal trim not only changes the airfoil angle of attack, but also, because of the elevon deflection, its shape. In order to obtain the flight polar, the elevon deflection for trim must be specified for each operating point. It is more convenient to define the deflection angle first and then use it as an input variable to derive the other parameters rather than the other-way around. The free-body diagram of the glider in longitudinal trim is presented in Fig. 11. For a given elevon deflection, the trim conditions can be expressed as,

$$L = W \qquad (6)$$

$$L \cdot x + M = 0 \qquad (7)$$

The first expression is based on the assumption that the angle of attack is small, such that the contribution of drag in the vertical direction is neglected.

The non-dimensional form of Eq. 7 is obtained by dividing both sides of the equality with the product of the dynamic pressure, the reference area, and the mean aerodynamic chord. This gives,

$$C_L = -C_M \cdot \left(\frac{\bar{c}}{x} \right) \tag{8}$$

Once a positive zero lift moment of sufficient magnitude is obtained, the center of gravity is located to provide a static margin that ensures an adequate amount of negative pitching moment gradient.[2, 9] The static margin required for satisfactory flying qualities is based on those of existing sailplanes.[2]

For a tailless design, one of the most discerning points is the small amount of pitch damping, which is roughly only one tenth of that of conventional aircraft.[7, 21] This seems to be one contributor to cause of the *SB 13's* tendency toward pilot induced oscillations.[7] While some papers suggest the adoption of a static margin for tailless sailplanes as small as 1.35%,[22] the performance estimations of this project use values closer to those of the *SB13*, ranging from 6% to 10%.[1]

Trim conditions

To determine the static trim conditions of the sailplane, it is necessary to first calculate the neutral point and the moment coefficient, C_{Mnp}, at that location. Without major viscous effects, the latter parameter is constant throughout the entire range of the angle of attack.[23] Thus, for the flight range of interest, the calculation was performed using the *DWT* panel method in order to evaluate the contribution of the stabilizing fuselage. To do this, the elevon deflection is set and the resulting aerodynamic forces are predicted at several angles of attack. The moment coefficients at the longitudinal stations of 1m and 3m from the nose were determined. An example is shown in Fig. 12 for no elevon deflection. The intersection of the two lines yields the zero-lift moment coefficient. The neutral point for this configuration depends strongly on the elevon deflection, which is determined for each elevon deflection as the moment center location that results in the C_M vs. C_L curve having zero slope. This entire procedure must be repeated a number of times with different elevon deflections to determine how the values for C_{Mnp} and the neutral point depend on the elevon deflection (in degrees). It is found that,

$$C_{Mo} = -0.015 \cdot \delta_{elev} + 0.0243 \tag{9}$$

$$NP = -0.0014 \cdot \delta_{elev} + 2.475 \tag{10}$$

These two expressions are used to determine the neutral point and the C_{Mnp} for any particular elevon deflection. The positioning of the center of gravity is located such that the static margin is between 6% and 10%. The center of gravity cannot be moved forward without increasing the stall speed. A larger static margin also requires an increased upward (negative) deflection of the elevon to trim at the same airspeed. Because this decreases the effective camber of the airfoil, the value of C_{Lmax} that can be obtained is diminished. Balancing the two requirements of low stall speed and an adequate static margin, the negative limit of the elevon deflection range is taken to be *–4.3* degrees. For this elevon deflection, c_{lmax} of the airfoil is approximately *1.24* at a Reynolds number of 1.0×10^6. The center of gravity is then located such that the static margin at low speeds is about 7% and at high speeds about 6%. This change in static margin with airspeed is due to the neutral point variation as it depends on elevon deflection, as expressed in Eq. 10.

Once the stability parameters are defined, Eqs. 9 and 10 can be used to determine the trim value of lift coefficient at each elevon deflection by substituting them into Eq. 8. This gives,

$$C_{Ltrim} = \left(0.015 \cdot \delta_{elev} - 0.0243\right) \cdot \left(\frac{\bar{c}}{\left(-0.0014 \cdot \delta_{elev} + 2.475 - x_{cg}\right)} \right) \tag{11}$$

The trim velocity is calculated using the lift equation, along with the approximation that weight equals lift, to obtain,

$$V_{trim} = \sqrt{\frac{2 \cdot W}{\rho \cdot C_{Ltrim} \cdot S}} \tag{12}$$

The upper and lower velocity limits for the flight polar diagram are defined by the never-exceed and the stall speeds respectively.[13, 24-25] The never-exceed speed is based on values representative of existing gliders, since these figures involve structural requirements analysis that are not part of this effort. The never-exceed speed is taken as *200* km/h and the stall speed as *74* km/h for unballasted conditions.

After the operating airspeed range is established, the elevon deflection is incremented by small amounts to obtain lift coefficients and airspeeds within the range of interest, and the drag is calculated at the corresponding points to yield the speed polar. All of the above procedure is iterative, requiring a number of trial calculations to obtain an acceptable compromise between parameters such as C_{Lmax}, the static margin, and the wing area.

Performance analysis

Drag prediction

The profile drag of the wing was determined by summing the contributions from discretized spanwise panels. The Horstmann lifting-line code was used to determine the local lift coefficient at each panel, along with the overall k-factor necessary to determine the induced drag coefficient. The local lift coefficients are then used as an input parameter along with the local Reynolds number of each panel to calculate the local profile drag coefficient using the two-dimensional airfoil code, *XFOIL*.[12] Transition from a laminar to a turbulent boundary layer was taken as natural or through a laminar separation bubble, unless it was predicted to occur behind the elevon

hinge point, in which case transition was forced there, at 75% chord for the elevons and 70% for the rudders. The total profile drag due to the wing is the sum of the contributions from each panel, along with those due to the vertical tails.

Two methods are used to predict the skin friction drag of the fuselage, and the results compared to check for consistency. The first method approximates the fuselage as a flat plate.[26] The wetted area distribution along the longitudinal axis is calculated, and then the skin-friction coefficient formulae of the laminar and turbulent boundary layer applied in order to estimate the fuselage skin-friction drag. For this calculation, transition is fixed at 0.9m from the nose. The second method of estimating the fuselage skin friction drag makes use of a feature in the *DWT* software package.[10] On-body streamlines cover every panel of the fuselage. A two-dimensional boundary-layer analysis is performed along each streamline to calculate the value of the skin-friction drag coefficient. The resulting force of each panel is integrated to get the total skin-friction drag of the fuselage. The skin-friction drag was calculated at various airspeeds at sea-level atmospheric conditions. The results of the two approaches agree well enough to justify the use of the following polynomial to approximate the fuselage skin-friction drag,

$$D_f = 0.0096 \cdot V_{trim}^2 + 0.028 \cdot V_{trim} + 0.5521 \qquad (13)$$

In order to estimate the pressure drag, the lift due to the fuselage without wings is taken to be negligible. Thus, the fuselage geometry is analyzed using *XFOIL* in the same way as are the wing airfoils. The resulting pressure drag coefficients at different airspeeds give a set of data that can be approximated by a simple power function using Reynolds number as a variable, such that,

$$C_{DPfuse} = 12.437 \cdot Re_{fuse}^{-0.5721} \qquad (14)$$

The last drag component that must be taken into account was that due to the wing/body interference and other miscellaneous factors such as leakage.[2, 23] These drags are accounted for by increasing the sum of the other drag contributions by 3%.

Straight-flight performance

To get an appreciation of the theoretical performance of the *H02g*, its speed polar is presented along with that of the *Discus 2*, in Fig. 13. While the predicted advantage of the *H02g* is slight, it does give some indication that the combination of the low pitching moment, laminar-flow airfoil along with the stabilizing fuselage does allow for a design that appears to be competitive in terms of straight-flight performance.

Average cross-country speed

The average cross-country speed of the *H02g* is also calculated for different weather conditions. In terms of the gliding speed, the sink rate during glide, and the climb rate, the average cross-country speed is given by,[2]

$$V_{ACC} = \left(\frac{d}{h}\right) \cdot \left[\frac{V_c \cdot V_s}{(V_c + V_s)}\right] = \frac{V_g}{\left(1 + \left(\frac{V_s}{V_c}\right)\right)} \qquad (15)$$

The optimum glide speed between thermals is determined using McCready speed-to-fly theory:[2, 27]

Climb performance

In order to find the optimal climb rate for a given thermal, the minimum sink rate of the turning sailplane is determined for different turning radii, and these results are considered along with the velocity distribution of the rising air mass in the thermal. The distribution of the vertical velocity in the thermal is taken as parabolic and based on the model of Quast.[2] Equating the forces in the horizontal direction acting on the sailplane, as shown in Fig. 16, yields,[2]

$$\frac{mV^2}{R} = L \cdot \sin(\phi) \qquad (16)$$

which can be combined with the lift equation to obtain the lift coefficient required for a given steady-state turn,

$$C_{Lreq} = \frac{2 \cdot m}{(R \cdot \rho \cdot S \cdot \sin(\phi))} \qquad (17)$$

In addition, the weight, *W*, must be equal to the vertical component of the lift force, such that during a steady turn the flight speed is given by, [2]

$$V_{turn} = \sqrt{\frac{2 \cdot W}{(\rho \cdot S \cdot C_L \cdot \cos(\phi))}} \qquad (18)$$

The lift to drag ratio during constant turning flight is then given by

$$\frac{V_{turn}}{V_{sink \cdot turn}} = \frac{L_{req} \cdot \cos(\phi)}{D} = \frac{C_{Lreq} \cdot \cos(\phi)}{C_D} \qquad (19)$$

The drag coefficient is obtained from the flight polar calculated previously. Accordingly, the turning sink rate is,

$$V_{sink \cdot turn} = V_{turn} \cdot \left(\frac{C_D}{C_{Lreq}}\right) \cdot \frac{1}{\cos(\phi)} \qquad (20)$$

Taking into consideration the maximum lift coefficient as a constraint, it is possible to find the minimum sink rate for a given turning radius. Compilation of such data for varying radii results in a diagram, as shown in Fig. 15, which expresses the vertical sink rate of the sailplane in a steady turn. The

overall vertical velocity of the aircraft is summed with the thermal profile. The glider climbs when its sink rate is less than the vertical velocity of the air mass.

The resulting average cross-country speeds are expressed as contour plots as a function of thermal radius and core strength, with and without water ballast, and presented in Figs. 16 and 17, respectively. The differences of the velocities in terms of percentage from those of the *Discus 2* are presented in Figs. 18 and 19. These predictions demonstrate that the conceptual design has the potential to achieve performance levels that are comparable to those of the current competitors.

Conclusions and recommendations

The adoption of a fuselage with a stabilizing moment and a laminar-flow airfoil with a low pitching moment results in a predicted performance that is essentially equal to that of contemporary gliders. While the advantage is not great, the predictions indicate that the concept of the stabilizing fuselage for tailless aircraft has some potential. This concept might also find application in the development of ultra- and mirco-lite gliders. In particular, having no tailboom would be advantageous for aircraft that are foot launched.

Although the predicted performance is on a par with that of conventional modern sailplanes, some of the traditional disadvantages of the tailless configuration still persist. For example, the direction that elevons must be deflected to control airspeed is opposite to that of conventional performance flaps. This factor necessitates new ideas from the airfoil designer in order for this idea to be introduced into classes that allow flaps. Likewise, since the airfoil used in this project is the result of modifications of existing airfoils that were designed between the late 1960s and the mid 1980s, an airfoil specifically designed for a tailless aircraft, using current understanding and tools, offers the possibility of further gains. Elevon geometry and deflection should also be optimized to satisfy the operational requirements of the sailplane.

Not much consideration was given to the effect of the camberline shape over the elevon. The camberline bending concave upward on the control surface creates a hinge moment that induces a further pitch down moment as a response to increased airspeed. The result is a negative stick force gradient. This problem is solved usually by applying an additional downward reflex to the elevon camberline. Furthermore, while the chord ratio of the elevon in this project has been defined at 25%, an additional design iteration would reduce it somewhat. This might result in a small but significant change in the drag polar, as the position of the hinge line influences the chordwise location of the transition point.

Having no antecedent to the concept of a stabilizing fuselage, the design process proceeded by iteratively trying out ideas using the *DWT* panel code. Searching for a methodological approach by implementing a numerical optimization scheme to design the fuselage might significantly benefit the design procedure and provide insight on the aerodynamic qualities of such components.

Finally, the planform of the wing has a significant sweepback that may introduce crossflow effects that would significantly alter the wing aerodynamics. The behavior with regard to the crossflow near its wingtips needs to be studied further, using empirical methods and analytical tools that fully account for the effects on the boundary layer.

Acknowledgements

Valuable data on the *SB13* was provided by Götz Bramesfeld, Hans Jürgen Berns and others contacted by the latter.

References

1 Nickel, K., Wohlfart, M., *Tailless Aircraft in Theory and Practice*, Translated by E. M. T. Brown, AIAA Education Series, Washington D.C., 1994.

2 Thomas, F., *Fundamentals of Sailplane Design*, Translated by J. Milgram, College Park Press, College Park, 1999.

3 Collinge, G. B., "Is a Horizontal Tail Necessary?" *Sport Aviation*, April – November 1984.

4 Kroo, I. M., "Tailless Aircraft Design–Recent Experiences," *Aerodynamics and Aeroacoustics*, Edited by K.Y. Fung, March 1993.

5 Larrabee, E. E., "The Aerodynamic Design of Sailplane Tail Assemblies," Proceedings of the XVth OSTIV Congress, Rayskala, Finland, 1976.

6 Schürmeyer, C., Horstmann, K-H., "Development of Airfoil Sections for the Swept-Back Tailless Sailplane SB13," Proceedings of the XIX_{th} OSTIV Congress, Rieti, Italy, 1985.

7 Berns, H-J., "Flight Testing the SB13 Flying Wing," Society of Engineering Test Pilots, 1997.

8 Johnson, R. H., "A Flight Test Evaluation of the Genesis 2 Sailplane," *Soaring*, Vol. 64, No. 3, pp 14-20, March 2000.

9 Etkin, B., *Dynamics of Flight: Stability and Control*, 2nd Edition, John Wiley & Sons, New York, 1982.

10 Aerologic, Digital Wind Tunnel CMARC Users Manual, Aerologic, Los Angeles, CA, 2000.

11 Horstmann, K-H., "Ein Mehrfach-Traglinienverfahren und seine Verwendung für Entwurf und Nachrechnung nichtplanarer Flügelanordnungen," DFVLR, Institut für Entwurfsaerodynamik Braunschweig, DFVLR-FB 87-51, Braunschweig, Germany, 1987.

12 Drela, M., *XFOIL: Subsonic Airfoil Development System*, User's Guide, Cambridge, MA, c. 1989.

13 Schempp-Hirth Flugzeugbau GmbH, "Schempp-Hirth Flugzeugbau GmbH Homepage," Kirchheim/Teck, Germany, c. 2003.

14 Raymer, D. P., *Aircraft Design: A Conceptual Approach*, 3rd Edition, AIAA Education Series, Reston, VA, 1999.

15 Akaflieg Braunschweig, Wägeprotokoll der SB13 mit MOPROMA, Akaflieg Braunschweig, Braunschweig, Germany, 1996.

16 Maughmer, M. D., The Evolution of Sailplane Wing Design, AIAA 2003-2777, 2003.

17 Perkins, C. D., Hage, R. E., *Airplane Performance Stability and Control*, John Wiley & Sons, New York, 1949.

18 Nelson, R. C., 2e, *Flight Stability and Automatic Control*, McGraw-Hill, Boston MA, 1998.

19 Multhopp, H., "Aerodynamics of the Fuselage," NACA Technical Memorandum 1036, Washington D.C., December 1942.

20 Cone, C. D. Jr., "The Theory of Induced Lift and Minimum Induced Drag of Nonplanar Lifting Systems," NASA Technical Report 139, February 1962.

21 Jones, R. T., Notes on the Stability and Control of Tailless Airplanes NACA Technical Notes 837, Washington D.C. December 1941.

22 Mönnich, W., Dalldorf, L., "A New Flying Qualities Criterion for Flying Wings," AIAA-93-3668-CP, August 1993.

23 McCormick, B. W., *Aerodynamics, Aeronautics and Flight Mechanics*, McGraw-Hill, New York, 1979.

24 LS Flugzeugbau GmbH, LS8a Flight Manual, Rolladen-Schneider Flugzeugbau GmbH, Egelsbach, Germany, 2001.

25 Alexander Schleicher GmbH & Co., ASW 28 Flight Manual, Alexander Schleicher GmbH & Co., Poppenhausen, Germany, 2003.

26 Anderson, J. D., *Fundamentals of Aerodynamics*, 2nd Edition, McGraw-Hill, New York, 1991.

27 Reichmann, H., *Cross-Country Soaring*, SSA, Hobbs NM, 1993.

Table 1
Vertical tail parameters.

Sailplane	l_{VT} [m]	$l_{VT}S_{VT}$ [m^3]	V_{VT} [m^3]
SB13	1.45	0.98	**5.63**
Genesis 2	1.80	1.44	**5.59**
H02g	1.34	1.68	**5.69**

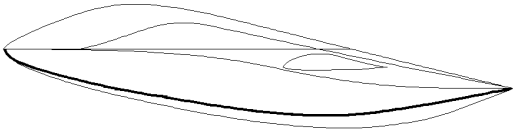

Figure 1 Fuselage maximum width line.

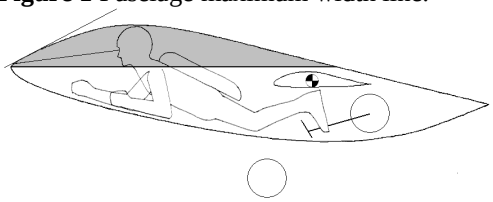

Figure 2 Pilot in prone position.

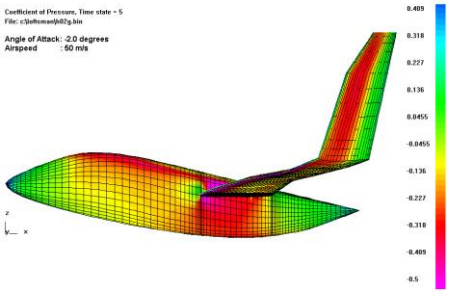

Figure 3 Side view of the pressure coefficient distribution.

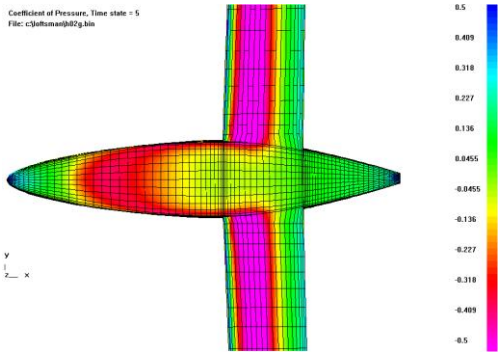

Figure 4 Top view of the pressure coefficient distribution.

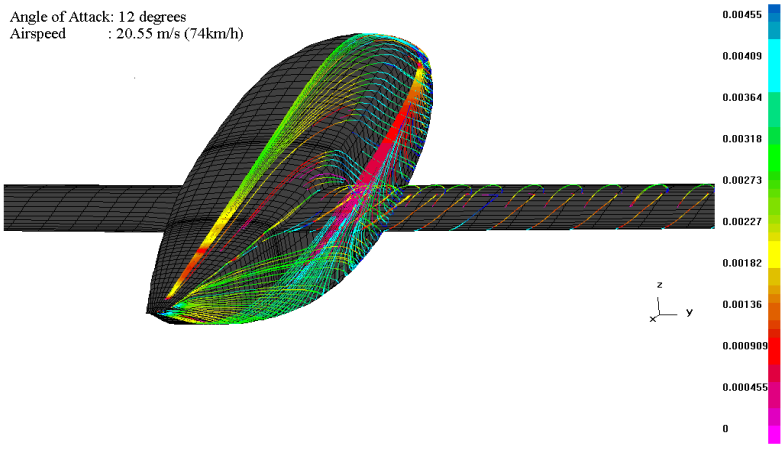

Figure 5 Flow separation prediction.

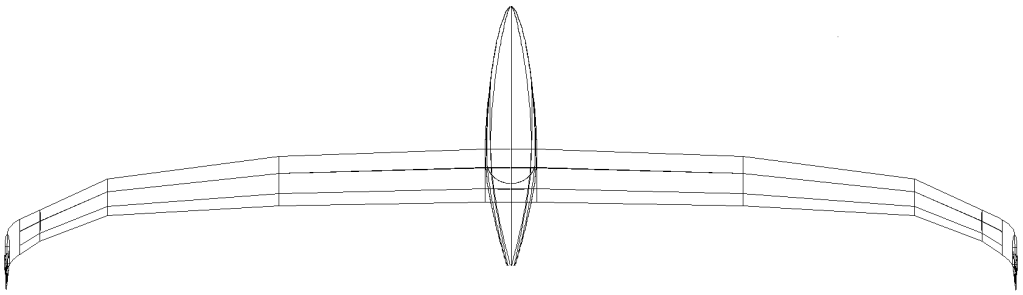

Figure 6 Top view of *HO2g* sailplane.

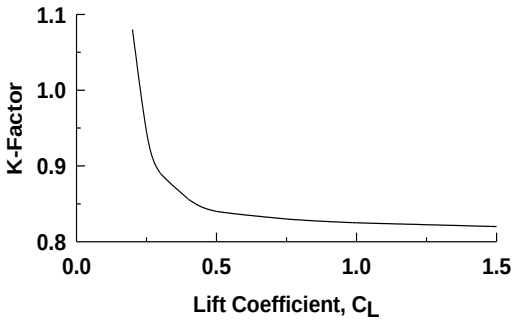

Figure 7 K-factor vs. lift coefficient.

Figure 8 Airfoil profile developed for main wing.

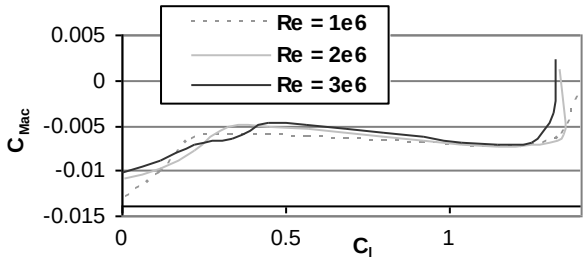

Figure 9 Moment coefficients about the aerodynamic center.

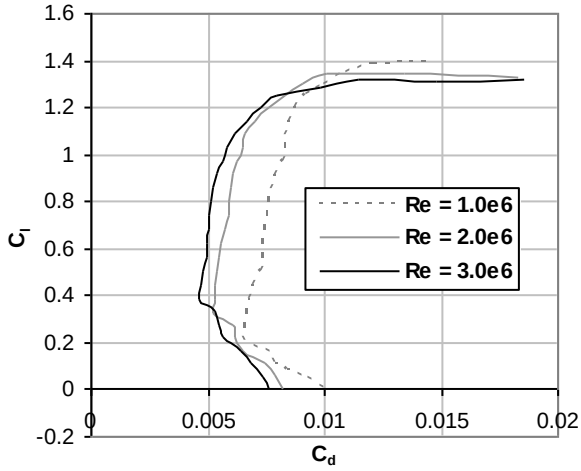

Figure 10 Airfoil drag polar.

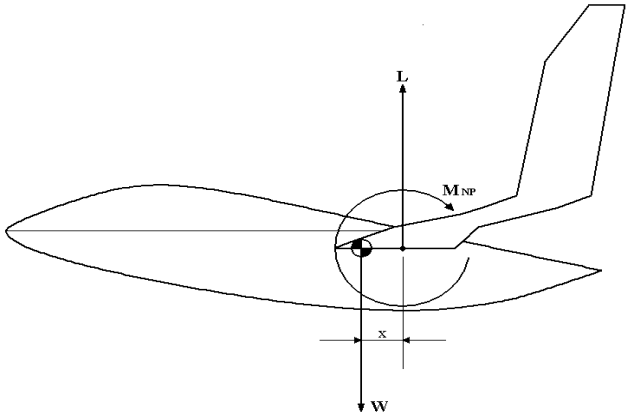

Figure 11 Free -body diagram of the glider.

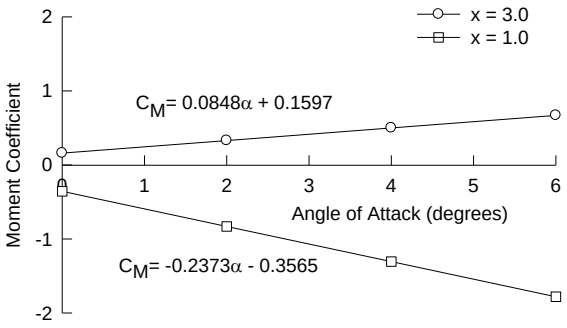

Figure 12 Moment coefficient vs. angle of attack**.**

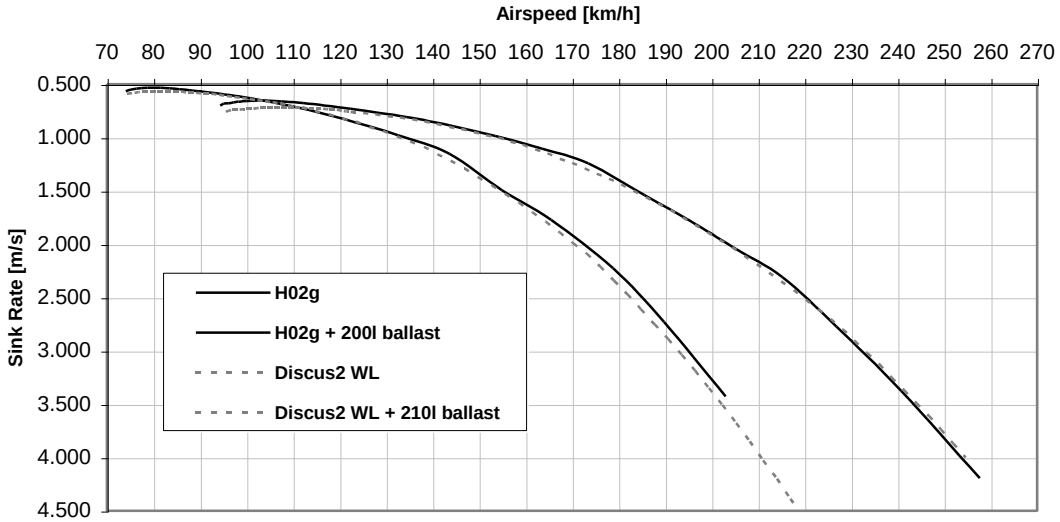

Figure 13 Flight polar diagram comparison with the *DiscusWL.*[13]

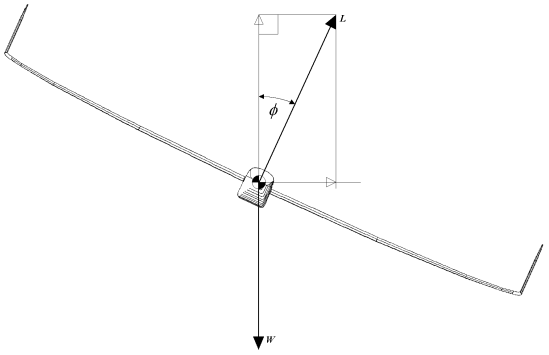

Figure 14 Free-body diagram (rearview) of a turning sailplane.

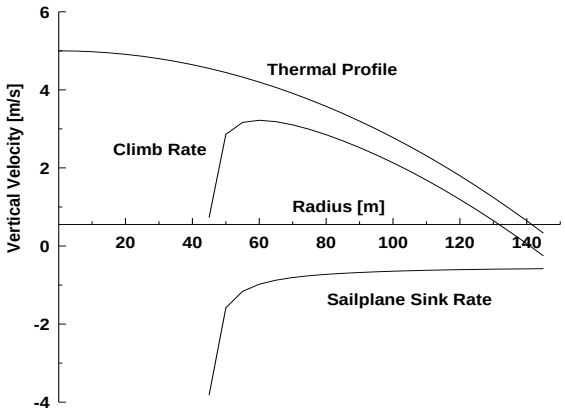

Figure 15 Climb rate diagram with a 150m radius thermal having 5m/s core strength.

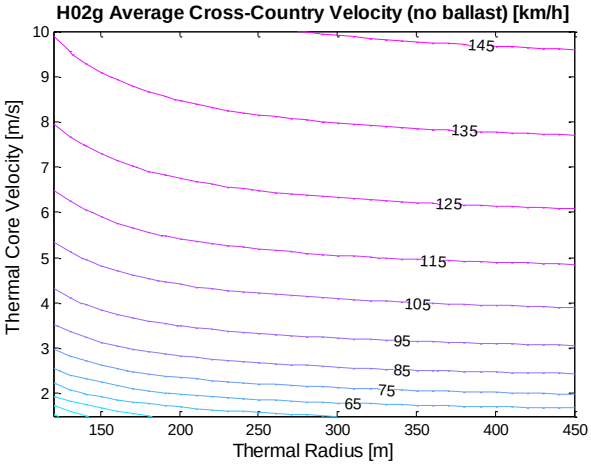

Figure 16 Average cross-country speeds with no ballast.

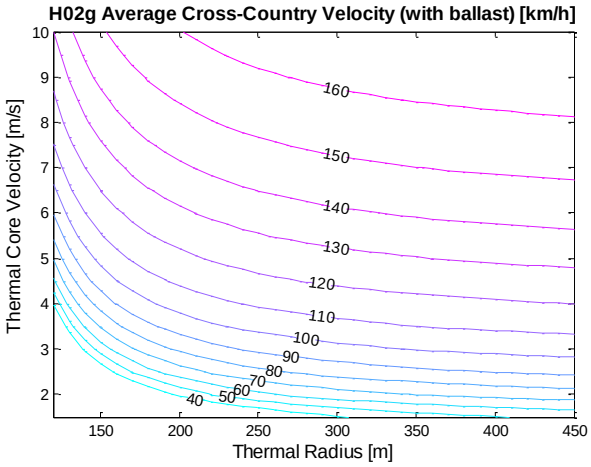

Figure 17 Average cross-country speed with full ballast.

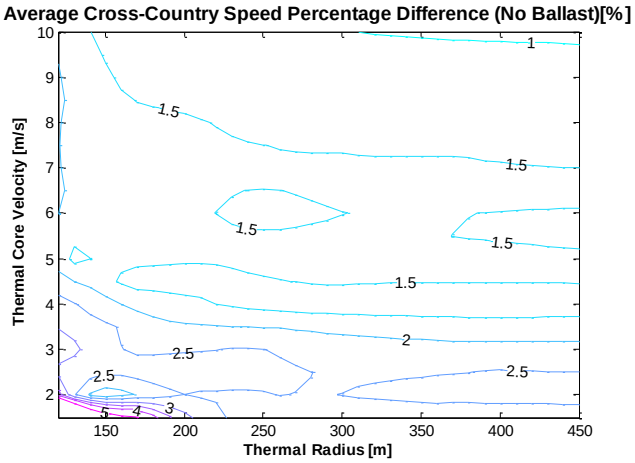

Figure 18 Average cross-country speed percentage improvement relative to the *Discus 2* (no ballast).

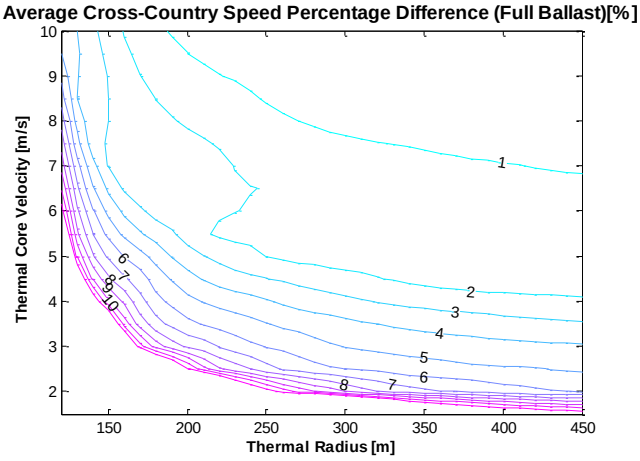

Figure 19 Average cross-country speed percentage improvement relative to the *Discus 2* (full ballast).